

Hydrogen super-saturated layers in H/D plasma loaded tungsten: a global model based on Thermodynamics, Kinetics and Density Functional Theory data

E. A. Hodille, N. Fernandez, Z. A. Piazza, M. Ajmalghan, and Y. Ferro*

*Laboratoire PIIM, Aix-Marseille Université/CNRS, Avenue escadrille Normandie-Niemen,
13397, Marseille, France*

Abstract

In this work, we combine Density Functional Theory data with a Thermodynamic and a kinetic model to determine the total concentration of hydrogen implanted in the sub-surface of tungsten exposed to a hydrogen flux. The sub-surface hydrogen concentration is calculated given a flux of hydrogen, a temperature of implantation, and the energy of the incoming hydrogen ions as independent variables. This global model is built step by step; an equilibrium between atomic hydrogen within bulk tungsten and a molecular hydrogen gas phase is first considered, and the calculated solubility is compared with experimental results. Subsequently, a kinetic model is used to determine the chemical potential for hydrogen in the sub-surface of tungsten. Combining both these models, two regimes are established in which hydrogen is preferentially trapped at either interstitial sites or in vacancies. We deduce from our model that the existence of these two regimes is driven by the temperature of the implanted tungsten sample; above a threshold or transition temperature is the *interstitial* regime, below is the *vacancy* regime in which super-saturated layers form within tenths of angstrom below the surface. A simple analytical expression is derived for the co-existence of the two regimes depending on the implantation temperature, the incident energy and the flux of the hydrogen ions which we use to plot the corresponding phase diagram.

*corresponding author: yves.ferro@univ-amu.fr

1. Introduction

The solubility of hydrogen in tungsten was experimentally established by Frauenfelder [1]; in the case of a tungsten sample in thermodynamic equilibrium with a hydrogen atmosphere, the solubility is around 10^{-18} *at.fr.* at room temperature and under standard pressure. Under low-energy hydrogen plasma exposure, the total amount of trapped hydrogen can rise to 10^{-2} *at.fr.* [2] or above [2-4]. Such a high solubility is reached despite the fact that the kinetic energy of the implanted ion is below the displacement threshold of the tungsten atoms, meaning that no radiation-defects are created to accommodate additional hydrogen atoms in tungsten. Consequently, the question of how the solubility can be increased by sixteen orders of magnitude under plasma exposure constitutes the central focus of the present paper.

It is known since the work of Fukai [5] that vacancies in metal can be created under a high pressure of hydrogen in the range of several GPa. On Pd and Ni, up to 20 *at.%* of vacancies were observed and this phenomena was consequently named Super-Abundant Vacancies (SAV). Each vacancy can individually accommodate one or multiple hydrogen atoms; they constitute traps for hydrogen and induce a dramatic increase of the solubility of hydrogen. Some thermodynamic models have been developed [6-11] since then to understand the formation of SAV in metals. The driving mechanism is that hydrogen decreases the formation energy of vacancies in the host metal, which results in the formation of a huge number of vacancies above a given pressure or chemical potential of hydrogen.

Such thermodynamic models have also been developed for tungsten [12-15]. The one of Sun et al. [12] is probably the most comprehensive; it gives the number of vacancies and the total solubility of hydrogen at a given chemical potential imposed by a H₂ atmosphere. Based on the previous work of Sugimoto [16], Sun et. al. [12] were able to relate the chemical potential to the pressure of the gaseous hydrogen far beyond ideal gas ranges up to GPas. However, the work of [12] does not take into account the temperature dependency of the many different

trapping energies and entropies of hydrogen in tungsten. In a previous work from us [13], the temperature dependency was introduced by including the vibrational energies and entropies for H in its multiple environments in tungsten: as interstitial (H_i), or in single vacancy (V) in which j H atoms can be trapped to form a VH_j vacancy with $j=0-12$.

During plasma exposure however, tungsten is not in contact with molecular hydrogen, but is exposed to a flux of hydrogen ions. As a consequence, the relation between the flux/energy of the plasma particles and the chemical potential of hydrogen must be established in order to predict the amount of hydrogen retained and the number of vacancies created into the tungsten material under various exposure conditions. To this end, we use the DFT data we recently published in [13] along with an improved thermodynamic model that includes the chemical potential of hydrogen. As a consequence, the equilibrium of the tungsten sample with a hydrogen reservoir of chemical potential μ can be described. In addition to this, a kinetic model recently proposed by Schmid *et al.* [3,17] is used to take into account the dependency of the flux and the ion energy of the particles during plasma exposure. Assuming a steady state is reached, a flux balance is established between diffusion into the sample of the implanted H/D atoms and outgassing from the sample. Combining both the results of the thermodynamic and kinetic model, we are able to determine a chemical potential from the ion energy and the flux of particles.

In the end, this global model allows to determine, within the implantation depth of tungsten, the atomic fractions of interstitial hydrogen, the overall concentration in vacancies and hydrogen trapped in vacancies under hydrogen exposure at a given temperature, flux and ion energy. The existence of two regimes is established: in a first one, hydrogen is trapped at interstitial sites, while in the second regime SAV are formed, which leads to hydrogen super-saturated layers (SSL). These SSL contain atomic fraction of hydrogen and vacancies in the range of the 1% at. fr., which is consistent with the experimental observations [2-4].

2. DFT data

The data needed to build the thermodynamic model were previously computed in ref [13] by means of electronic structure calculations using DFT with the Quantum Espresso code [18]. Based on these data, we calculated the formation energy of an interstitial hydrogen atom e_{int} in its lowest energy configuration (this occurs when hydrogen is located at tetrahedral position of the *bcc* unit cell of perfect tungsten), the formation energy of a single empty vacancy e_0 , and the formation energy of a single vacancy VH_j that traps j hydrogen atoms e_j :

$$e_{int} = E_{HW_n}^{DFT} - E_{W_n}^{DFT} - E_{H_{ref}}^{DFT} \quad (1)$$

$$e_0 = E_V^{DFT} - \frac{n-1}{n} E_{W_n}^{DFT} \quad (2)$$

$$e_j = e_V + E_{VH_j}^{DFT} - E_V^{DFT} - j E_{H_{ref}}^{DFT} \quad (3)$$

where $E_{W_n}^{DFT}$ is the electronic energy of a unit-cell containing $n=54$ atoms in ref [13], $E_{HW_n}^{DFT}$ is the energy of the same unit-cell with a hydrogen atom in a tetrahedral position, E_V^{DFT} is the energy of the single vacancy (i.e. the unit-cell with one W atom removed), $E_{VH_j}^{DFT}$ is the energy of a single vacancy incorporating j H atoms, with $j=1$ to 12 , and $E_{H_{ref}}$ is a reference energy of hydrogen. $E_{H_{ref}}^{DFT}$ can be chosen as the energy of atomic hydrogen or half the energy of a hydrogen molecule. As we are only dealing with energy difference, this reference energy will cancel out anyway. We nevertheless used half the energy of a H_2 molecule to calculate e_{int} , e_0 and e_j displayed in Table 1. These data are in good agreement with some other ones that can be found in the literature [19-21]. For $j = 1$ to 6 , the formation energy of a VH_j vacancy requires less energy than the formation of an empty vacancy e_0 ; this energy difference is indeed the driving mechanism that leads to the formation of abundant VH_j vacancies.

Sites	Energies (eV)
e_{int}	0.93
e_0	3.25
e_1	2.99
e_2	2.73
e_3	2.57
e_4	2.54
e_5	2.57
e_6	2.83
e_7	3.48
e_8	4.08
e_9	4.81
e_{10}	5.60
e_{11}	6.58
e_{12}	7.20

Table 1: formation energies e_{int} of an interstitial atom, e_0 of an empty single vacancy, and e_j of a single-vacancy filled with j H atoms as calculated from equations 1, 2 and 3.

The Gibbs free energy was further computed using the phonon properties of hydrogen in tungsten calculated via Density Functional Perturbation Theory (DFPT) [22] while keeping all the tungsten atoms frozen. This was also previously done in Ref [13] and was proven to be valid due to the mass difference of hydrogen and tungsten. The Gibbs free energy *per* particles g_{ints} and g_j were computed with following equation:

$$g = (e^{DFT} + h^{vib}) - Ts^{vib} \quad (4)$$

The formula for h^{vib} and s^{vib} are given in the Appendix. g_V is simply e_V since we neglected the phonon properties of the tungsten network. The standard free energy *per* particle of H₂ in the gas phase was also calculated, which requires adding the translational and rotational components of enthalpy and entropy to the equation (4). At standard pressure P° , $g_{H_2}^\circ$ is determined according to:

$$g_{H_2}^\circ = (e_{H_2}^{DFT} + h_{H_2}^{vib} + h_{H_2}^{rot} + h_{H_2}^{trans}) - T(S_{H_2}^{vib} + S_{H_2}^{rot} + S_{H_2}^{trans}) \quad (5)$$

Again, the translation and rotational component to the chemical potential are given in the Appendix. Until the ideal gas law is verified, the Gibbs free energy of H₂ is given by:

$$g_{H_2} = g_{H_2}^\circ + k_B T \ln \sqrt{\frac{P}{P^\circ}} \quad (6)$$

The range of validity of this model is however limited by the temperature: phonons are computed in the quasi-harmonic approximation, which limits the range of temperature to below 1000K, after which anharmonic effects should be considered [23].

3. Thermodynamic and kinetic models

In the following we present the different steps used to build the global model. In a first step, perfect tungsten is considered in equilibrium with a H₂ atmosphere near standard pressure; in such conditions the ideal gas law can be applied and no SAV are formed; a thermodynamic model is built to determine the solubility of hydrogen in these experimental conditions. The model is validated against the experimental data on hydrogen solubility from Frauenfelder [1]. In a second step, single-vacancies are added to the model while an equilibrium with a H₂ gas phase is still considered. The total solubility of hydrogen at interstitial sites or trapped in vacancies is determined as a function of the temperature and the pressure. In a third step, a relation between the energy and flux of the impinging ions and the concentration of hydrogen located at interstitial sites is established via a kinetic model. With the concentration of hydrogen at interstitial sites established, we are then able to determine the chemical potential of hydrogen within the range of its implantation depth and consequently, we determine the solubility of hydrogen along with the number of created vacancies.

3.1 - Hydrogen solubility in perfect W

We herein consider a tungsten sample in equilibrium with a H_2 atmosphere at pressure P and temperature T . In a grand-canonical-ensemble picture, the reservoir is the H_2 atmosphere containing N_H hydrogen atoms (i.e. $N_H/2$ hydrogen molecules). The system is the tungsten sample in which n_{int} hydrogen are retained at interstitial sites. N_H is so huge as compared to n_{int} that it can be considered as constant. As a consequence, the pressure of the reservoir is constant and the chemical potential it imposes to the system is constant too. On the contrary, n_{int} varies up to the point where equilibrium with the reservoir is established. A schematic representation of such a model is given in the table below.

	H_2 (Reservoir)	H_{int} (System – W)
<i>Initial</i>	$\frac{1}{2}N_H$	0
<i>Equilibrium</i>	$\frac{1}{2}(N_H - n_{int})$	n_{int}

The relevant physical quantity to study such an equilibrium is the Gibbs free energy of the system, which is simply the sum of the Gibbs free energy *per* particle of each constituent of the system *plus* a configurational term:

$$G = \frac{1}{2}(N_H - n_{int})g_{H_2} + n_{int}g_{int} - T S_{conf} \quad (7)$$

$$S_{conf} = k_B \ln \left[\frac{\gamma N!}{(\gamma N - n_{int})! n_{int}!} \right] \quad (8)$$

The configurational entropy expresses all of the configurations that can be built when placing n_{int} hydrogen atom into the *bcc* lattice of a tungsten sample of N W atoms; $\gamma = 6$ is the number of tetrahedral interstitial site in the *bcc* structure of tungsten. The chemical potential μ of H in the reservoir is $\mu = \frac{1}{2}g_{H_2}(P, T)$. The equilibrium conditions being given by $(\frac{\partial G}{\partial n_{int}})_{T,P} = 0$,

the atomic fraction $x_{int} = \frac{n_{int}}{N}$ or solubility of hydrogen in tungsten at equilibrium with a reservoir of chemical potential μ is then :

$$x_{int} = \frac{\gamma}{1 + \exp\left(\frac{g_{int} - \mu}{k_B T}\right)} \quad (9)$$

Unless $x_{int} < 10^{-2}$ at.fr., $\exp\left(\frac{g_{int} - \mu}{k_B T}\right)$ is large in comparison to 1 and the previous equation simplifies to:

$$x_{int} = \gamma \exp\left(-\frac{g_{int} - \mu}{k_B T}\right) \quad (10)$$

$$x_{int} = \gamma \sqrt{\frac{P}{P^\circ}} \exp\left(-\frac{g_{int} - \frac{1}{2} g_{H_2}^\circ}{k_B T}\right) \quad (11)$$

Equation (11) uses the chemical potential of molecular hydrogen assuming an ideal behavior. It is also known as the Sievert's law, which has been measured experimentally by Frauenfelder [1] for tungsten at high temperature between 1100K and 2400K. In this range of temperature, impurities and other defects are supposed to have only insignificant effects on the solubility itself.

Considering a reservoir at the standard pressure P° , the results from equation (11) are plotted on Figure 1 between room temperature and around 1000K. An extrapolation of the Frauenfelder's law $x_{int} = 9.3 \times 10^{-3} \exp\left(-\frac{1.04}{k_B T}\right)$ at low temperature is provided in Figure 1. The error bars given by Frauenfelder are also used to define the upper and lower boundaries for the solubility within the experimental uncertainty. Using these data, we were able to plot the lower boundary x_{int}^{B-} (or bottom of the error bars) over the full range of temperature according to $x_{int}^{B-} = 5.10 \times 10^{-3} \exp\left(-\frac{1.21}{k_B T}\right)$, and the upper boundary x_{int}^{B+} (or

top of the error bars) over the full range of temperature according to $x_{\text{int}}^{\text{B}+} = 1.82 \times 10^{-2} \exp\left(-\frac{0.87}{k_{\text{B}}T}\right)$.

The agreement between the calculated and experimental solubility is excellent in the range of temperature considered as can be seen from Figure 1. The same model will consequently be used in the next section to determine the hydrogen solubility in tungsten with vacancies.

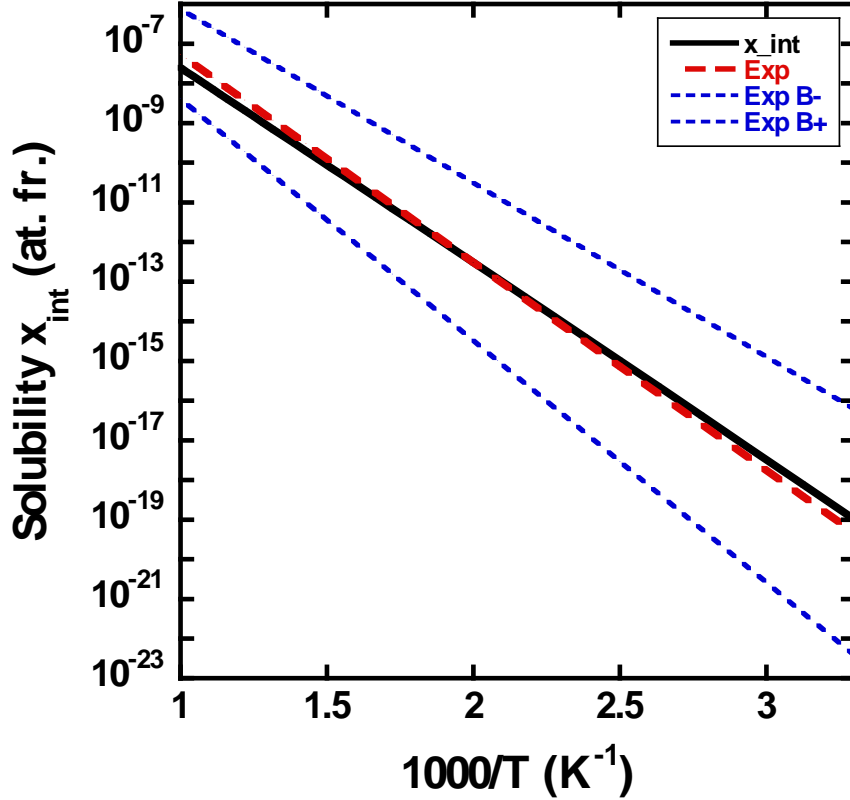


Figure 1: Calculated solubility x_{int} (black line) compared to the experimental solubility measured by Frauenfelder (red dashed line). Also, the error bars given by Frauenfelder are plotted (blue dotted lines).

3.2 - Hydrogen solubility in tungsten with single vacancies

A reservoir of N_H atoms in the form of H_2 molecules and temperature T and pressure P is again used to impose the chemical potential $\mu = \frac{1}{2}g_{\text{H}_2}(P, T)$ to the system. We now consider the case in which the pressure is in the range of GPa. At such a pressure, single-vacancies are

created in large number and have to be taken into account into the model. The number of vacancies that trap j H atoms is n_j , and the total amount of hydrogen trapped in the single vacancies is $n_{trapped} = \sum_{j=0}^{12} j n_j$. The total number of H atoms absorbed in the sample is n_H and the total number of vacancies is n_v :

$$n_H = n_{int} + \sum_{j=0}^{12} j n_j \quad (12)$$

$$n_v = \sum_{j=0}^{12} n_j$$

All n_j , n_{int} , n_H and n_v vary as in the previous paragraph up to the point where the equilibrium is reached. The atomic fraction x_j , x_H , x_{int} and x_v (same quantities but divided by the number N of W atoms) will be equally used throughout this paper. A schematic representation of such a system is given by the table below.

	(Reservoir)	(System – W)	
	H ₂	H _{int}	H _{vac}
<i>Initial</i>	$\frac{1}{2}N_H$	0	0
<i>Equilibrium</i>	$\frac{1}{2}(N_H - n_H)$	$n_{int} = n_H - \sum_{j=0}^{12} j n_j$	$\sum_{j=0}^{12} j n_j$

The Gibbs free energy of the whole system is:

$$G = \frac{1}{2}(N_H - n_H)\mu_{H_2} + n_{int} g_{int} + \left(\sum_{j=0}^{12} j n_j g_j \right) - T S_{conf} \quad (13)$$

$$S_{conf} = k_B \ln Z_{int}^{conf} + k_B \ln Z_{vac}^{conf}$$

$$Z_{int}^{conf} = \frac{\gamma N!}{(\gamma N - n_{int})! n_{int}!} \quad Z_{vac}^{conf} = \frac{(N - n_v)!}{n_v!} \prod_{j=0}^{12} \frac{\omega_j^{n_j}}{n_j!} \quad (14)$$

ω_j is the number of degenerate configurations in which j H atoms are located in a single vacancy and was taken from Ref [14]. The equilibrium conditions are now given by

$$\left(\frac{\partial G}{\partial n_j}\right)_{T,P,n_i \neq n_j} = 0 \text{ and } \left(\frac{\partial G}{\partial n_{int}}\right)_{T,P} = 0.$$

The first condition leads to:

$$\frac{x_j}{\omega_j(1+x_v)} \left(\frac{\gamma-x_{int}}{x_{int}}\right)^j = \exp\left(-\frac{g_j-j g_{int}}{k_B T}\right) \quad (15)$$

while the second condition leads to equation 9 again. Combining equations (9) and (15) gives:

$$\frac{x_j}{1+x_v} = \omega_j \exp\left(-\frac{g_j-j \mu}{k_B T}\right) \quad (16)$$

Noticing that $\sum_{j=0}^{12} x_j = x_v$, one finally gets:

$$x_j = \frac{1}{C} \omega_j \exp\left(-\frac{g_j-j \mu}{k_B T}\right) \quad (17)$$

$$C = 1 - \sum_{j=0}^{12} \omega_j \exp\left(-\frac{g_j-j \mu}{k_B T}\right)$$

In cases such as $x_v \ll 1$, then $C \approx 1$ and equation (17) takes a very simple analytical form.

Equations (9) or (10) and (17) can now be used to determine the atomic fraction of interstitial H atoms and the atomic fraction of H atoms trapped in vacancies, respectively, provided that the chemical potential μ is known. The limit of validity of this model is reached at a concentration around 10^{-2} at. fr. (1%) of vacancies. At such a concentration, traps interact with each other, thus the trapping energies for hydrogen are modified as compared to the corresponding trapping energies for diluted vacancies in tungsten. Moreover, aggregation of vacancies and the formation of vacancy clusters is expected. Also, the configurational entropy will take a more complex form as discussed in [13]. This limit is however set at a very high concentration and the domain of validity of the model is consequently quite robust.

3.3 - Kinetic model

The objective of this sub-section is to determine the chemical potential μ as a function of the implantation conditions, and consequently all the properties and behavior of hydrogen within tungsten. This can be achieved using equations (10) or (11), provided that the fraction of interstitial H atoms x_{int} is known. Based on a simple kinetic model, an analytical expression for x_{int} was recently proposed in Ref [3,17].

In this model, an incident flux ϕ_{inc} ($m^{-2}s^{-1}$) of ions with energy E_{inc} (eV) is assumed to create a triangular depth-profile of interstitial hydrogen atoms in tungsten as represented in Figure 2.

The implanted flux is $(1 - r) \cdot \phi_{inc}$ where r is the dimensionless reflection coefficient of the ions and depends on the incident energy E_{inc} of the ions. R_p is the mean depth of ion implantation and is also dependent on E_{inc} . The fraction of hydrogen remains maximal at the peak depth over time since the flux of ions continuously implants particles to this depth. This maximal fraction of interstitial hydrogen is called x_{int}^{MAX} . The migration of the hydrogen atoms from the implantation zone to the bulk is characterized by the distance $R_d(t)$.

Regarding the profile from R_p to a position which is deeper into the bulk in Figure 2, the linear shape can be justified as follows. If diffusion dominates over trapping, the fraction of diffusive interstitial hydrogen x_{int} at depth d is known [24]; it is $x_{int}(d, t) = x_{int}^{MAX} \operatorname{erfc}\left(\frac{d}{2\sqrt{D(T)t}}\right)$, in which $D(T)$ (m^2s^{-1}) is the diffusion coefficient of interstitial hydrogen. Such a profile is plotted with dashed line in Figure 2. Due to the presence of traps, the erfc shape of $x_{int}(x, t)$ is modified and becomes almost linear as shown by macroscopic rate equation and finite element simulations of H in W [25]. This justifies the linear shape we used in our simple kinetic model.

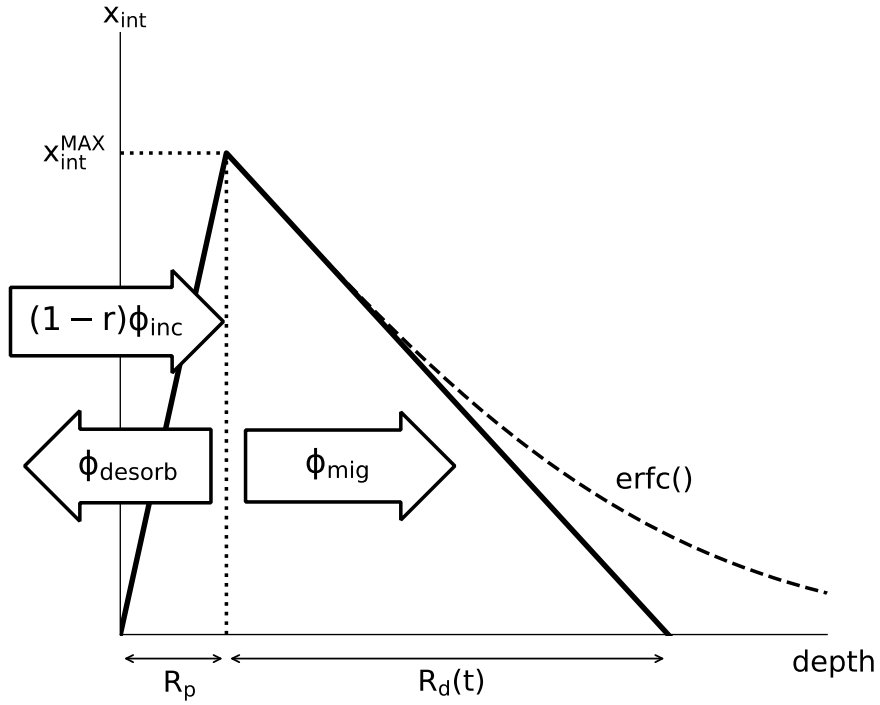


Figure 2: Schematic representation of the depth profile of interstitial hydrogen atoms x_{int} during an implantation with H^+/D^+ ions. The profile is shown from the surface (left) to the bulk (right).

According to Fick's law of diffusion, these two fluxes depend on the diffusion coefficient of hydrogen in tungsten $D(T)$:

$$\phi_{desorb} = D(T) \cdot \frac{x_{int}^{MAX} \cdot \rho_W}{R_p} \quad (18)$$

$$\phi_{mig} = D(T) \cdot \frac{x_{int}^{MAX} \cdot \rho_W}{R_d(t)}$$

Where $\rho_W \approx 6.18 \times 10^{28} \text{ at.m}^{-3}$ is the tungsten density. The flux balance between the desorbing flux, the migration flux and the implanted flux yields:

$$(1 - r) \cdot \phi_{inc} = -\phi_{desorb} + \phi_{mig} \quad (19)$$

The distance $R_d(t)$ shown in Figure 2 increases with time. ϕ_{mig} is inversely proportional to $R_d(t)$; In a semi-infinite material, it consequently decreases and tends towards zero with time. In a real material of finite length L_0 , $R_d(t)$ will obviously stop once hydrogen reaches the opposite surface, such that $L_0 = R_d + R_p$. The thickness of a W sample is typically around

100 μm . Considering implantation energies of tens to hundreds eV, a typical value for R_p as $R_p \approx 10 \text{ nm}$, and following equations (18), we have $\frac{\phi_{mig}}{\phi_{desorb}} \approx 10^{-4}$. It means that even though ϕ_{mig} does not reach zero in a finite sample, ϕ_{mig} is negligible as compared to ϕ_{desorb} and can be neglected in equation (19). As a consequence, when the steady state is reached, the implantation and desorption fluxes equilibrate, which leads to:

$$x_{\text{int}}^{\text{MAX}} = R_p \cdot \frac{(1 - r) \cdot \phi_{\text{inc}}}{D(T) \cdot \rho_W} \quad (20)$$

All the quantities are known in equation (20) since ϕ_{inc} is given by the experimental conditions, $D(T) = D_0 \exp\left(-\frac{E_a}{kT}\right)$ is the diffusion coefficient calculated by DFT [13], and R_p and r can be easily determined via the binary collision approximation Monte Carlo code SRIM (Stopping and Range of Ions in Matter) [26,27]. SRIM needs E_{inc} as input data, which is also given by the experimental conditions. In Appendix II, the conditions within which a steady state is reached are investigated. Combining equations (9) or (10), (18) and (20) yields the chemical potential of hydrogen, the total solubility of hydrogen and the defect concentration created in the material at R_p , which we examine in the next sub-section.

4. Super-saturation in tungsten

4.1 – Global model

The kinetic and thermodynamic model are herein combined to yield an estimate of the hydrogen concentration implanted in the sub-surface of tungsten around R_p at a given implantation temperature. The sub-surface is indeed the range of validity of the model; since we use a thermodynamic model, an equilibrium has to be established at least locally. The sub-surface layer is located where the energy of the implanted ions is deposited and thus acts as an

energy bath for the system in this region. Consequently, kinetic processes are easily activated in this region, which ensures that equilibrium is reached, and the model applies.

In a first step we model the fraction of hydrogen implanted in the sub-surface. We apply the kinetic model with implantation conditions commonly found in the literature: $\phi_{\text{inc}} = 10^{19} \text{m}^{-2} \text{s}^{-1}$ and $E_{\text{inc}} = 500 \text{ eV/ion}$. The reflection coefficient r and mean depth of implantation were given by SRIM are $r = 0.51$ and $R_p = 7.7 \text{ nm}$. The kinetic model allows us to determine $x_{\text{int}}^{\text{MAX}}$ given in equation 20, and then to determine the chemical potential μ from equation 10. The fraction x_j of VH_j vacancies in the sub-surface layers are subsequently calculated using equations (18). These fractions are plotted in Figure 3 in a range of temperature from 300K to 800K.

The most populated vacancies are the VH_6 for an implantation at 300K, followed by VH_7 and VH_5 , then VH_4 up to V_0 . This ranking is inverted at higher temperature, namely at 800K. The same qualitative trend exists when an equilibrium with a H_2 gas phase is considered [13]; however in the case of implantation, the concentration of vacancies and the solubility of hydrogen dramatically increases to $x_V = 0.4\%$ and $x_H = 2.4\%$ at 300K. This result is in good agreement with experimental observations that report the formation of super-saturated layers (SSL) within the first ten nanometers of tungsten after implantation at room temperature [3]. It also follows that these SSL would be a consequence of SAV which drastically increase the hydrogen concentration while simultaneously inducing a huge number of defects.

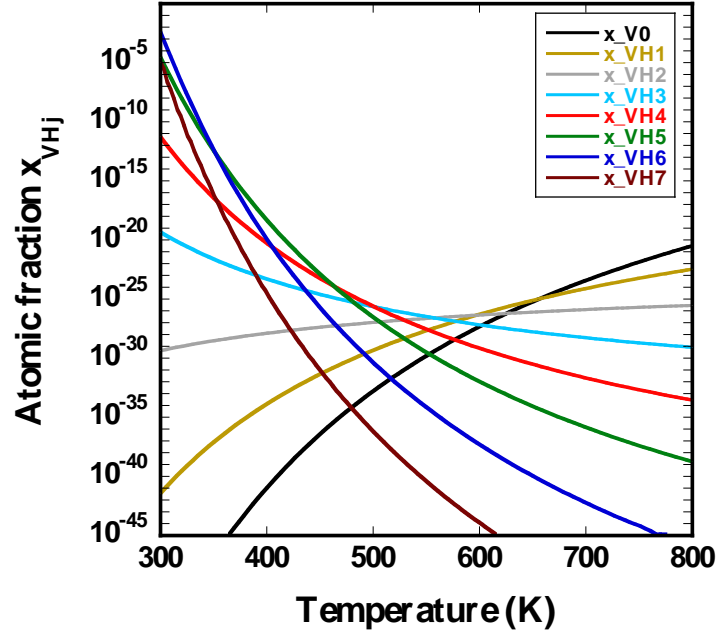


Figure 3: Atomic fraction of VH_j vacancies in the sub-surface layer of tungsten within 10 nm with a flux $\phi_{inc} = 10^{19} \text{m}^{-2} \text{s}^{-1}$ and ion energy $E_{inc} = 500 \text{ eV/ion}$.

To better understand the formation mechanism of the supersaturated layers, we plotted in Figure 4 the total fraction of hydrogen implanted in the sub-surface as a function of the temperature. This was done for fluxes ranging from $\phi_{inc} = 10^{17} \text{m}^{-2} \text{s}^{-1}$ to $\phi_{inc} = 10^{24} \text{m}^{-2} \text{s}^{-1}$ and for an incident energy $E_{inc} = 500 \text{ eV/ion}$. Two regimes are observed; at high temperatures, the total solubility of hydrogen varies slowly with temperature and remains within one order of magnitude; the concentration is mostly dependent on the flux of implantation. At low temperatures, the total solubility dramatically increases as the temperature decreases; SSL are consequently formed in this regime. The dotted lines in Figure 4 display the fraction of hydrogen trapped at interstitial sites only (i.e. the fraction of hydrogen located within vacancies is removed). It is clear that the dramatic increase in the hydrogen solubility is the consequence of the formation of vacancies in huge numbers that accommodate hydrogen atoms. As a consequence, the physical distinction between these two regimes is driven by trapping at interstitial sites at high temperature, and by the formation of SAV and trapping of hydrogen in the form of VH_j vacancies at low temperature. Our model

predicts that the formation of SAV and consequent trapping of VHj vacancies in the low temperature regime is what causes the formation of the experimentally observed SSL.

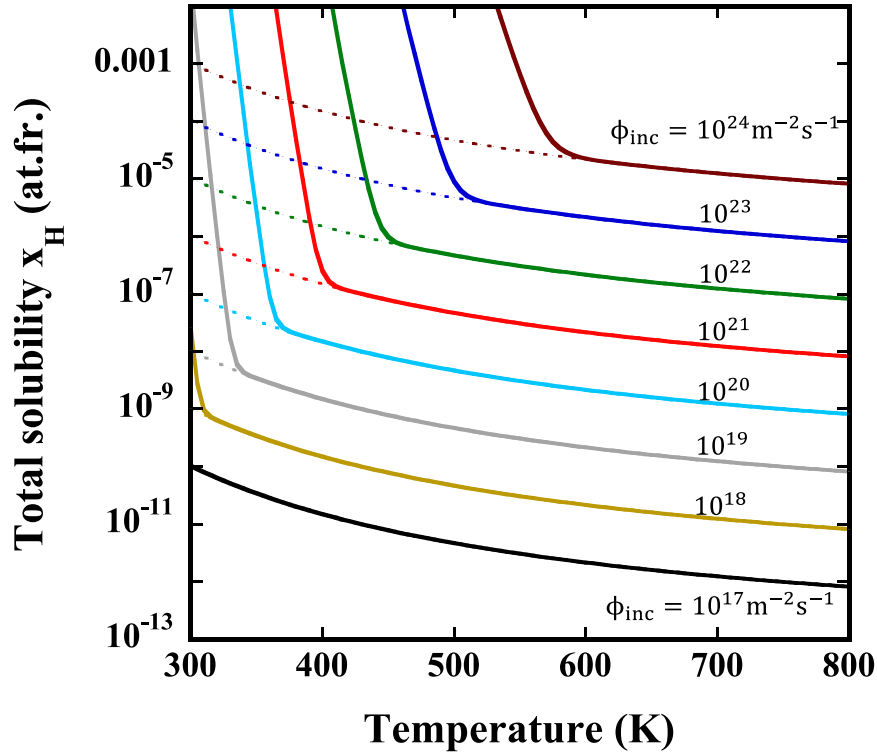


Figure 4: Total solubility of hydrogen (bold lines) implanted at Rp for various incident fluxes ranging from $\phi_{inc} = 10^{17} \text{m}^{-2} \text{s}^{-1}$ to $\phi_{inc} = 10^{24} \text{m}^{-2} \text{s}^{-1}$ plotted as a function of the temperature of implantation and for an incident energy of $E_{inc} = 500 \text{ eV/ion}$. The fraction of hydrogen trapped at interstitial sites is also plotted in dotted lines for comparison.

In summary, the temperature of transition between the *vacancy* and *interstitial* regimes depends on the flux: while the *vacancy* regime is not reached at room temperature for a flux of $\phi_{inc} = 10^{17} \text{m}^{-2} \text{s}^{-1}$, it is reached below 550K with a flux of $\phi_{inc} = 10^{24} \text{m}^{-2} \text{s}^{-1}$. This temperature of transition T_t is clearly seen in Figure 4 and corresponds to the points where the total solubility and the solubility at interstitial sites are no longer superimposed. Once again, the domain of validity of the present model is in the sub-surface layer where the energy of the implanted ions is deposited. Deeper into the bulk, high concentrations of hydrogen are also

measured and were found around 10^{-4} *at.fr.* [2,4]. The thermodynamic model remains the same deeper into the bulk, but the formation and diffusion of vacancies are kinetically hindered. The activation energies for diffusion are 1.7eV and 2.1eV for VH_0 and VH_1 , respectively [13].

4.2 – Temperature of transition depending on the flux

Below, a simple analytical expression is established for the transition temperature between the *interstitial* and the *vacancy* (or SSL) regimes. At T_t , the fraction of hydrogen trapped in interstitial sites x_{int} is equal to the fraction of hydrogen trapped in vacancies. It was already shown [13, 14, 19] that the most populated vacancies at room temperature are VH_6 ; This can be seen in Figure 3 where the population of VH_6 dominates by two to three orders of magnitude over VH_7 and VH_5 . This leads to the condition $x_{int} = j x_j$ with $j = 6$.

Equation 10 and 17 with $C = 1$ allows to determine the transition temperature depending on the chemical potential:

$$T_t = \frac{1}{k_B \ln \frac{\gamma}{j \omega_j}} [g_{int} - g_j + (j - 1)\mu] \quad (21)$$

The chemical potential is determined using equation (10) and (20):

$$\mu = E_a + g_{int} + k_B T_t \ln \left[\frac{R_p(1 - r) \cdot \Phi_{inc}}{\gamma \rho_W D_o} \right] \quad (22)$$

The transition temperature depending on the flux is the determined combining equations (21) and (22):

$$T_t = \frac{g_j - j g_{int} - (j - 1)E_a}{k_B \left[(j - 1) \ln \left[\frac{R_p(1 - r) \cdot \Phi_{inc}}{\gamma \rho_W D_o} \right] + \ln \frac{j \omega_j}{\gamma} \right]} \quad (23)$$

T_t can be plotted easily assuming that $g_{int} \approx e_{int} = 1.18$ eV when corrected from the Zero Point Energy (ZPE), $g_j \approx e_j = 4.08$ eV also corrected from the ZPE with $j = 6$ (using $j=5$ and

$e_5=3.60\text{eV}$ does not significantly affect the result). The activation energy for diffusion is $E_a = 0.20\text{ eV}$, the other quantities in equation 23 are $D_0 = 1.9 \cdot 10^{-7}\text{ m}^2\text{s}^{-1}$, $\gamma = 6$, $\omega_6 = 1$ and $\rho_W = 6.18 \times 10^{28}\text{ at.m}^{-3}$. In the end, R_p and r are determined by the incident energy E_{inc} of the ion. They are given by SRIM : $r=0.51$ and $R_p = 7.7\text{ nm}$ at $E_{\text{inc}} = 500\text{ eV}$, and $r=0.56$ and $R_p = 2.4\text{ nm}$ at $E_{\text{inc}} = 70\text{ eV}$.

T_t is plotted in Figure 6 for E_{inc} equal to 500eV and 70eV. T_t agrees well with the one that can be read on Figure 5 with $E_{\text{inc}} = 500\text{ eV}$. As a consequence, equation 23 gives a simple and easy to use analytical expression that allows one to predict the experimental conditions leading to the formation of hydrogen super-saturated layers in tungsten: the SSL are formed in conditions corresponding to the top left of Figure 5, while on the right-hand side no SSL is formed. Figure 6 can be read as a diagram of existence of the SSL.

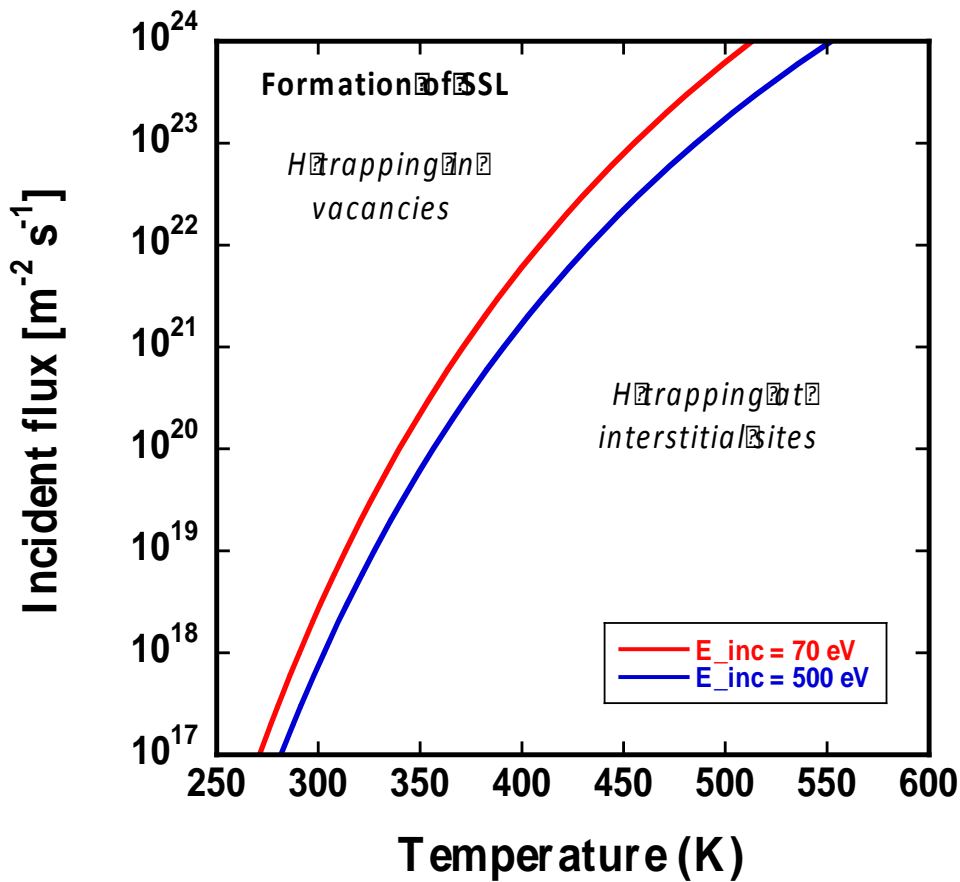


Figure 5: Diagram of existence of the SSL: temperature of transition between the interstitial and vacancy regime for hydrogen trapping plotted as a function of the incident flux of the ions for 2 incident energies, $E_{inc}=500\text{eV}$ as in Figure 5, and $E_{inc} = 70\text{eV}$.

Even if this phase diagram still needs to be validated against experimental results, we can nevertheless compare with the results from Gao et al [3] recorded at $T=300\text{K}$ with $E_{inc} = 70\text{eV}$ and $\phi_{inc} = 9.910^{-19} \text{ m}^{-2}\text{s}^{-1}$. With these experimental conditions, they fall in the SSL domain in good correspondence with the concentration experimentally determined to 9.4% *at.fr*. In addition, Poon et al. [28], studied the retention of D in a single crystalline sample implanted by 500 eV/D ions at 300 K and various fluxes; they reported a significant decrease of the deuterium retention for fluxes below $1 \times 10^{18} \text{ m}^{-2}\text{s}^{-1}$; this would indicate that the coordinate $T=300\text{K}$, $\phi_{inc} = 1.0 \times 10^{-18} \text{ m}^{-2}\text{s}^{-1}$ lies on the transition curve, which is clearly the case in Figure 4 and 5, and would consequently be in full agreement with the model.

5. Conclusion

In this work we combined DFT data, a kinetic model, and a thermodynamic model to produce a global model enabling us to examine the behavior of hydrogen in tungsten under hydrogen ions irradiations. The results of our model provide the data to construct a simple diagram allowing one to predict the domain of existence of the super-saturated layers depending on the flux, the energy of the ions, and the temperature of implantation of hydrogen in tungsten. A simple analytical expression is given for the temperature of transition between the *interstitial* and *vacancy* regimes, which make it easy to determine the experimental conditions leading to the formation of the SSL.

Acknowledgment

First of all, we would like to express gratitude to our Slovenian and German colleagues for

the fruitful discussions and scientific exchanges we had about the contents of this work:

S. Markelj from JSI, K. Shmid, T. Schwarz-Selinger, A. Manhard, L. Gao and S. Kasper from IPP Garching.

This work was carried out within the framework of the EUROfusion Consortium and received funding from the Euratom research and training programme 2014-2018 under grant agreement No 633053 and also the A*MIDEX project (n° ANR-11-IDEX-0001-02) funded by the ‘Investissements d’Avenir’ French Government program, managed by the French National Research agency (ANR). The views and opinions expressed herein do not necessarily reflect those of the European Commission. The authors of this work were granted access to the HPC resources of IDRIS and CINES under the allocation A0020806612 made by GENCI (Grand Equipement National de Calcul Intensif) and to the Marconi Supercomputer at CINECA Super Computing Application and Innovation Department, Bologna, Italy.

Appendix

Appendix I

The vibrational enthalpies and entropies were calculated as follows:

$$h_{vib} = \sum_{j=1}^{n_{vib}} h\nu_j \left(\frac{1}{2} + \frac{1}{\exp\left(\frac{h\nu_j}{k_B T}\right) - 1} \right) \quad (\text{AI-1})$$

$$s_{vib} = k_B \sum_{j=1}^{n_{vib}} \left[\frac{h\nu_j}{k_B T} \frac{1}{\exp\left(\frac{h\nu_j}{k_B T}\right) - 1} - \ln \left(1 - \exp\left(-\frac{h\nu_j}{k_B T}\right) \right) \right] \quad (\text{AI-2})$$

For the gas phase, it is also necessary to consider the translational and rotational components to the Gibbs free energy. Since H_2 is a homonuclear diatomic molecule, these components were computed as follows:

$$h_{trans} = \frac{5}{2} k_B T \quad s_{trans}^{\circ} = k_B \left(\frac{5}{2} + \ln \left[\frac{k_B T}{P^{\circ}} \left(\frac{2 \pi m k_B T}{h^2} \right)^{\frac{3}{2}} \right] \right) \quad (\text{AI-3})$$

$$h_{rot} = k_B T \quad s_{rot} = k_B \left(1 + \ln \left[\frac{8 \pi^2 I k_B T}{\sigma h^2} \right] \right) \quad (\text{AI-4})$$

In s^{rot} , σ depends on the symmetry of the molecule. It is 2 for a homonuclear diatomic molecule. I is the inertia momentum of H_2 .

Appendix AII

We herein check the conditions within which the steady state leading to equation [15] is reached. To this end, we assume the concentration of trapped hydrogen is constant up to the depth $R_d(t)$. This concentration of trapped hydrogen is called $x_{trapped}$. It follows the number

of hydrogen trapped per surface unit is $c_{trapped} = \rho_w R_d(t) x_{trapped}$. The flux which is feeding the growth of this quantity is ϕ_{mig} . It came that, $\phi_{mig} = \frac{d c_{trapped}}{dt}$. Taking the expression of ϕ_{mig} from equation (18), this leads to $R_d(t) dR_d(t) = \frac{D(T)}{x_{trapped}} x_{int}^{MAX} dt$, which is $R_d(t) = \sqrt{\frac{2D(T)x_{int}^{MAX}}{x_{trapped}}} t$ once integrated over time. Using this expression in the flux balance (13)

$$0 = \frac{D(T)}{R_p} \cdot \left(\sqrt{x_{Hi}^{MAX}} \right)^2 + \sqrt{\frac{x_{Htrapped} \cdot D(T)}{2 \cdot t}} \cdot \sqrt{x_{Hi}^{MAX}} - (1 - r) \cdot \frac{\phi_{inc}}{\rho_w} \quad (\text{AII-1})$$

we end up with:

$$\sqrt{x_{int}^{MAX}} = \sqrt{R_p \cdot \frac{(1 - r) \cdot \phi_{in}}{D(T) \cdot \rho_w}} \cdot \sqrt{\frac{\tau_m}{t}} \cdot \left(\sqrt{1 + \frac{t}{\tau_m}} - 1 \right) \quad (\text{AII-3})$$

Where $\tau_m = \frac{R_p \rho_w x_{trapped}}{8(1-r)\phi_{inc}}$ is the time characterizing the growth of x_{int}^{MAX} . Figure A shows the evolution of $x_{int}^{MAX}/x_{int}^{MAX}_{t \rightarrow \infty}$ as a function of t/τ_m as described by equation (14). It requires $t = 360\tau_m$ for x_{int}^{MAX} to reach 90% of its steady-state value defined by the equation (20) which can be considered as the steady-state condition. In experiment, a typical implantation flux is $(1 - r)\phi_{inc} = 10^{19} Dm^{-2}s^{-1}$ with ion energy of 250 eV/D. This ion energy, at normal incidence, leads to $R_p = 5 nm$. Considering $10^{-2} at.fr$ as an upper limit for $x_{trapped}$, one can obtain $\tau_m = 0.0425 s$. Thus, the steady-state condition is $t > 15.3 s$. Considering the experimental runs last for hundreds or even thousands of seconds to reach fluence $> 1021 Dm^{-2}$, it appears very reasonable to assume that the steady-state is reached during experiments.

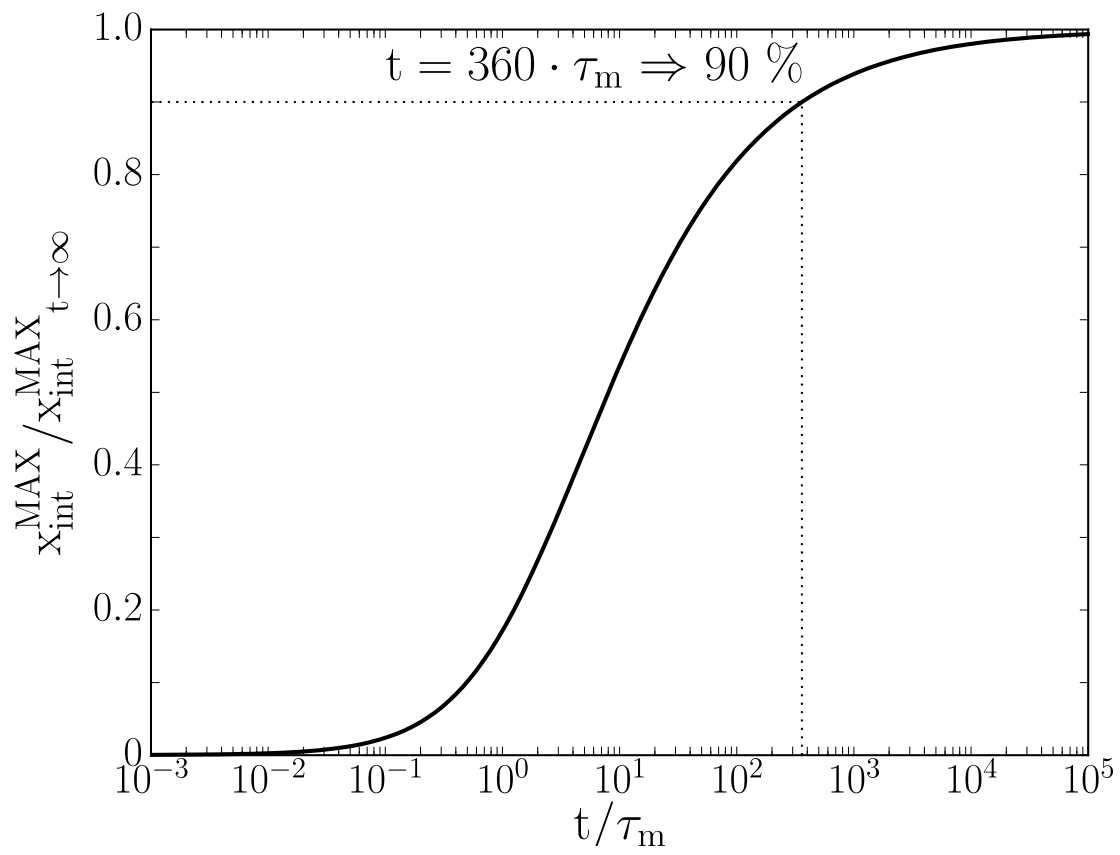


Figure A: evolution of x_{int}^{MAX} with time t/τ_m .

Bibliography

- [1] R. Frauenfelder, Solution and diffusion of hydrogen in tungsten, *Journal of Vacuum Science and Technology*, 6 (1969) 388.
- [2] V. K. Alimov, J. Roth and M. Mayer, Depth distribution of deuterium in single- and polycrystalline tungsten up to depths of several micrometers, *J. Nucl. Mater.* 337-339 (2005) 619-623.
- [3] L. Gao, W. Jacob, U. von Toussaint, A. Manhard, M. Balden, K. Schmid and T. Schwarz-Selinger, Deuterium supersaturation in low-energy plasma-loaded tungsten surfaces, *Nucl. Fusion* 57 (2017) 016026.
- [4] J. Roth, T. Schwarz-Selinger, V.Kh. Alimov, and E. Markina. Hydrogen Isotope Exchange in Tungsten: Discussion as Removal Method for Tritium. *Journal of Nuclear Materials* 432 (2013) 341–47.
- [5] Y. Fukai, N. Okuma, Formation of Superabundant Vacancies in Pd Hydride under High Hydrogen Pressures, *Phys. Rev. Lett.* 73 (1994) 1640–1643
- [6] Y. Fukai, Formation of superabundant vacancies in M–H alloys and some of its consequences: a review, *Journal of Alloys and Compounds* 356–357 (2003) 263–269
- [7] A. Metsue, A. Oudriss, X. Feugas, Hydrogen solubility and vacancy concentration in nickel single crystals at thermal equilibrium: New insights from statistical mechanics and ab initio calculations, *Journal of Alloys and Compounds* 656 (2016) 555-567
- [8] D. Tanguy, Y. Wang, D. Connetable, Stability of vacancy-hydrogen clusters in nickel from first-principles calculations, *Acta Materialia* 78 (2014) 135–143
- [9] D. Connetable, M. David, A. Prillieux, D. Young, D. Monceau, Impact of the clusterization on the solubility of oxygen and vacancy concentration in nickel: A multi-scale approach, *Journal of Alloys and Compounds* 708 (2017) 1063-1072
- [10] R. Nazarov, T. Hickel, and J. Neugebauer, First-principles study of the thermodynamics of hydrogen-vacancy interaction in fcc iron, *Phys. Rev. B* 82 (2010) 224104
- [11] Min Ji, Cai-zhuang Wang, and Kai-ming Ho, Statistical model of defects in Al-H system, *Physical Review B*, 81(2010) 024105,
- [12] L. Sun, S. Jin, H.B. Zhou, Y. Zhang, W. Zhang, Y. Ueda, H. T. Lee and G. H. Lu, Critical concentration of hydrogen bubble formation in metals, *J. Phys.: Condens. Matter* 26 (2014) 395402
- [13] N. Fernandez, Y. Ferro and D. Kato, Hydrogen diffusion and vacancies formation in tungsten: Density Functional Theory calculations and statistical models, *Acta Materialia*, 94 (2015) 307-318
- [14] K. Ohsawa, F. Nakamori, Y. Hatano, M. Yamaguchi, Thermodynamics of hydrogen-induced superabundant vacancy in tungsten, *Journal of Nuclear Materials* 458 (2015) 187–197

- [15] D. Kato, H. Iwakari, Y. Watanabe, K. Morishita and T. Muroga, *Nuclear Fusion* 55 (2015) 083019, Super-saturated hydrogen effects on radiation damages in tungsten under the high-flux divertor plasma irradiation
- [16] H. Sugimoto and Y. Fukai, Solubility of hydrogen in metals under high hydrogen pressures: Thermodynamical calculations, *Acta. Metall. Mater.* 40 (1992) 2327
- [17] K. Schmid, Diffusion-trapping modelling of hydrogen recycling in tungsten under ELM-like heat loads, *Phys. Scr.* T167, p. 014025, 2016
- [18] P. Giannozzi, S. Baroni, N. Bonini, M. Calandra, R. Car, C. Cavazzoni, Davide Ceresoli, G.L. Chiarotti, M. Cococcioni, I. Dabo, A.D. Corso, S. de Gironcoli, S. Fabris, G. Fratesi, R. Gebauer, U. Gerstmann, C. Gougoussis, Anton Kokalj, M. Lazzeri, L. Martin-Samos, N. Marzari, F. Mauri, R. Mazzarello, Stefano Paolini, A. Pasquarello, L. Paulatto, C. Sbraccia, S. Scandolo, G. Sclauzero, A.P. Seitsonen, A. Smogunov, P. Umari, R.M. Wentzcovitch, QUANTUM ESPRESSO: a modular and open-source software project for quantum simulations of materials, *J. Phys. Condens. Matter.* 21 (2009) 395502. doi:10.1088/0953-8984/21/39/395502.
- [19] K. Ohsawa, J. Goto, M. Yamakami, M. Yamaguchi, M. Yagi, Trapping of multiple hydrogen atoms in a tungsten monovacancy from first principles *Phys. Rev. B* 82 (2010) 184117.
- [20] Y.W. You, X.S. Kong, X.B. Wu, Y.C. Xu, Q.F. Fang, J.L. Chen, et al. Dissolving, trapping and detrapping mechanisms of hydrogen in bcc and fcc transition metals, *AIP Adv.* 3 (2013) 012118.
- [21] Y. L. Liu, Y. Zhang, H-B. Zhou, and G-H Luo, *Phys. Rev. B* 79 (2009) 172103, vacancy trapping mechanism for hydrogen bubble formation in metal.
- [22] S. Baroni, S. de Gironcoli, A. Dal Corso, P. Giannozzi, Phonons and related crystal properties from density-functional perturbation theory, *Rev. Mod. Phys.* 73 (2001) 515–562. doi:10.1103/RevModPhys.73.515.
- [23] A. Glensk, B. Grabowski, T. Hickel, J. Neugebauer, Breakdown of the Arrhenius law in describing vacancy formation energies: the importance of local anharmonicity revealed by ab initio thermodynamics, *Phys. Rev. X*, 4 (2014) 011018
- [24] J. Crank, *The Mathematics of Diffusion*, Oxford University Press, London and New York 1957
- [25] S. Benannoune, Y. Charles, J. Mougnot, M. Gaspérini, Numerical simulation of the transient hydrogen trapping process using an analytical approximation of the McNabb and Foster equation, *International Journal of Hydrogen Energy*, 43, (2018), 9083-9093
- [23] www.srim.org.
- [24] J.F. Ziegler, M.D. Ziegler, Biersack J.P., SRIM-the stopping and range of ions in matter (2010), *Nucl. Inst. Methods Phys. Res. B* 268 (2010) 1818-1823
- [25] M. Poon, A.A. Haasz, J.W. Davis, R. G. Macaulay-Newcombe, Impurity effects and

temperature dependence of D retention in single crystal tungsten J. of Nucl. Mater. 313-316
(2003) 199